CRYSTAL GROWTH & DESIGN

Article

pubs.acs.org/crystal

Effect of Crystal Habit on Intrinsic Dissolution Behavior of Celecoxib Due to Differential Wettability

Sameer R. Modi,[†] Ajay K. R. Dantuluri,[†] Sathyanarayana R. Perumalla,[‡] Changquan Calvin Sun,[‡] and Arvind K. Bansal*,[†]

[†]Department of Pharmaceutics, National Institute of Pharmaceutical Education and Research (NIPER), SAS Nagar, Punjab 160062, India

[‡]Department of Pharmaceutics, College of Pharmacy, University of Minnesota, 308 Harvard Street S.E., Minneapolis, Minnesota 55455-0343, United States

ABSTRACT: Intrinsic dissolution rate (IDR) is a useful technique to differentiate the solid forms of a drug. In the present study, the impact of crystal habit and crystal size on IDR of celecoxib (CEL) in different media was assessed. The IDR of plate-shaped CEL crystals (CEL-P) (53.4 ± 6.7 μg/min/cm^2) was 46.3% higher than that of acicular crystals (CEL-A) (36.5 ± 1.7 μg/min/cm^2) in pH 12 phosphate buffer. Contact angle experiments and values of dispersive and polar components of surface free energy indicated better wettability of CEL-P compacts than CEL-A. Higher IDR and better wettability of CEL-P were attributed to favorable exposure of hydrophilic crystal facets on compact surface, due to preferred orientation during compaction. In contrast to native samples, milled CEL-A (MCEL-A) and milled CEL-P (MCEL-P) showed similar IDR. Interestingly, IDR of CEL-A (36.5 ± 1.7 μg/min/cm^2) and MCEL-A (35.64 ± 5.09 μg/min/cm^2) did not show any significant difference ($p > 0.05$). However, IDR of CEL-P (53.4 ± 6.7 μg/min/cm^2) was significantly higher ($p < 0.05$) than that of MCEL-P (39.15 ± 2.48 μg/min/cm^2). This was ascribed to (i) differential cleavage behavior of CEL-A and CEL-P during milling and (ii) reduced degree of preferred orientation of hydrophilic facets in MCEL-P compacts. This work provides an interesting case study of the impact of particle level properties and surface molecular environment on IDR.

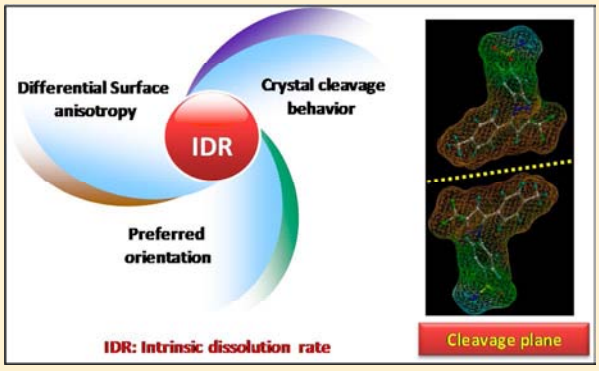

1. INTRODUCTION

The solid form of an active pharmaceutical ingredient (API) has considerable impact on its physicochemical properties and subsequent product performance. Different solid forms arising from changes in either internal structure or external appearance are manifested as polymorphs and crystal habit, respectively.[1,2]

Material science tetrahedron (MST) describes a relationship between structure, property, processing, and performance of materials.[3] The concept of quality by design (QbD) stresses understanding the relationship between material properties and product performance. Within this framework, many reports have focused on studying the impact of polymorphs on pharmaceutical performance.[4−15] Another interesting, though less studied, area is the role of crystal habit on processing and performance, such as tabletability, dissolution, and oral bioavailability.[16−21]

It is often preferable that the dissolution rate is expressed in terms of a surface specific value (i.e., in μg/min/cm^2) for understanding the role of different solid forms on the biopharmaceutical performance of an API. This can be achieved by monitoring the change in surface area as a function of time during powder dissolution or by exposing a constant surface area of the dissolving solid,[22] which can be achieved using an intrinsic dissolution assembly, e.g., Wood's assembly.[23−27] Both normalization of the powder dissolution rate by surface area and dissolution using a disc with a fixed surface area can give the intrinsic dissolution rate (IDR). In this work, we have adopted the disc IDR approach.

Many studies had demonstrated differential wetting behaviors of different crystalline facets,[9,10,14,28] which is responsible for their facet-specific dissolution behaviors.[8,13] For acetaminophen crystals that differ in habit, the surface normalized powder dissolution rate varies with habit but the disc IDR does not.[29] Although it has been speculated that crystal habit may affect disc IDR of a given solid form,[4,8,30] convincing experimental evidence has been lacking in the scientific literature.

We had previously shown that crystal habit modification of celecoxib (CEL) influences its powder dissolution profile and oral bioavailability because of the anisotropic surface chemistry of crystal habits and differences in relative abundance of various crystal facets.[18] These results suggest that CEL might be a good

Received: July 19, 2014
Revised: August 31, 2014

   dx.doi.org/10.1021/cg501084a | *Cryst. Growth Des.* XXXX, XXX, XXX−XXX

model compound for probing the effect of crystal habit on disc IDR. In the present study, we compared disk IDR of acicular and plate-shaped crystals of CEL form III, with and without milling, and the results were correlated with their differential surface properties.

2. EXPERIMENTAL SECTION

2.1. Materials. Form III Celecoxib (CEL, Figure 1), chemically designated as 4-[5-(4-methyl-phenyl)-3-(trifluoromethyl)-1*H*-pyrazol-1-yl] benzenesulphonamide (assay value >99%), was received as a gift from Dr. Reddy's Laboratories Ltd. (Hyderabad, India). Toluene (Merck, India), ethanol (Merck, India), ethylene glycol (EG, Merck, India), and diiodomethane (DIM, Sigma-Aldrich, Germany) were of high performance liquid chromatography (HPLC) grade. All other chemicals used were of analytical grade.

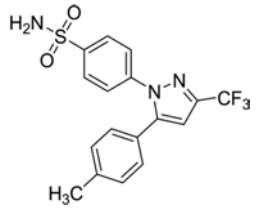

Figure 1. Molecular structure of CEL.

2.2. Crystallization of Different Crystal Habits. Acicular and plate-shaped habits of CEL were crystallized from toluene by varying the degree of supersaturation and crystallization temperature.[17,18] Briefly, an accurately weighed amount (about 200 mg) of drug was dissolved in 10 mL of toluene at 72 °C. The hot solution was immediately filtered into a glass beaker using 0.22 μm nylon filters and cooled to either 25 or 60 °C to achieve 190% and 102% supersaturation, respectively. The degree of supersaturation was calculated from solution concentration and predicted solubility at the target temperature based on a van't Hoff plot previously constructed.[18] Acicular crystals (CEL-A) were obtained when the solution with 190% degree of supersaturation was evaporated at 25 °C. Plate-shaped crystals (CEL-P) were generated when the solution with 102% degree of supersaturation was evaporated at 60 °C. The crystals were collected after 72 h and dried under a vacuum at room temperature. The two different crystal habits of CEL were sieved through British sieve size (BSS) No. 52 and retained on BSS No. 100 to minimize the particle size variations.

The two crystal habits were also milled using a mortar and pestle and sieved through BSS 400. Henceforth, milled fractions of CEL-P and CEL-A are mentioned as MCEL-P and MCEL-A. Both the unmilled and milled fractions of the two habits were characterized for their solid state properties.

2.3. Optical and Polarized Light Microscopy. CEL crystals were characterized for their crystal habit and aspect ratio by measuring length along the longest axis and width of 200 individual particles using a Leica DMLP polarized light microscope (Leica, Germany). Cumulative Particle Size Distribution (PSD) curves were plotted to determine the diameters corresponding to 10%, 50%, and 90% of cumulative undersize particles, i.e., D_{10}, D_{50}, and D_{90}.

2.4. Preparation of Compacts. Powder samples (200 mg) were compacted using an 8 mm punch die set, at 6.9 MPa pressure in a hydraulic press (Hydraulic Unit model 3912, Carver Inc., WI), with a dwell time of 60 s. Porosity of the compacts calculated using eq 1 was 0.22 ± 0.02, 0.20 ± 0.03, 0.18 ± 0.03, and 0.18 ± 0.02 for CEL-A, CEL-P, MCELA, and MCEL-P, respectively ($p > 0.05$).

$$\varepsilon = 1 - \rho_c/\rho_t \quad (1)$$

where ρ_c is the density of the compact calculated from the weight and volume of the resulting compact and ρ_t is the true density of crystalline powder determined by helium pycnometry (Pycno 30, Smart Instruments, India).

2.5. Scanning Electron Microscopy (SEM). The surface morphology of all powder samples and their compacts was viewed using a scanning electron microscope (S-3400, Hitachi Ltd., Tokyo, Japan) operated at an excitation voltage of 25 kV. Samples were mounted onto steel stage using double-sided adhesive tape and coated with gold 133 using ion sputter (E-1010, Hitachi Ltd., Tokyo, Japan) before the analysis.

2.6. Differential Scanning Calorimetry (DSC). Thermal analysis of all powder samples and their compacts was carried out to determine melting point and heat of fusion using DSC (TA Instruments Q2000, New Castle, Delaware, USA) equipped with TA Universal Analysis software. The instrument was calibrated for heat flow and temperature with high purity indium. CEL crystals and small portions of compacts (about 3−5 mg) were weighed into a crimped aluminum pan and analyzed at a heating rate of 20 °C/min over a temperature range of 35−200 °C with nitrogen purging (50 mL/min). All measurements were performed in triplicate.

2.7. Thermogravimetric Analysis (TGA). The presence of solvent or any degradation during heating was examined using TGA/SDTA (model 851e, Mettler Toledo, Switzerland) operated with Stare software (version Solaris 2.5.1). Accurately weighed (5−10 mg) samples were loaded into alumina crucibles and heated at a heating rate of 20 °C/min over a temperature range of 35−200 °C, under nitrogen purge (50 mL/min), to determine weight loss. All measurements were performed in triplicate.

2.8. X-ray Powder Diffractometry (XRPD). XRPD patterns of all powder samples and their compacts were recorded at room temperature using a X-ray diffractometer (model D8 Advance, Karlsruhe, West Germany) equipped with a 2θ compensating slit, using Cu−Kα radiation (1.54 Å) at 40 kV and 40 mA passing through nickel filter with divergence slit (0.5°), antiscattering slit (0.5°) and receiving slit (0.1 mm). Samples were mounted on polymethyl methacrylate (PMMA) sample holder and subjected to a continuous scan over 3−40° 2θ at a step size of 0.01° and a dwell time of 1 s/step. Diffractograms were analyzed with DIFFRAC^{plus} EVA (version 9.0) diffraction software. Peak intensities (net area) were determined by integrating the area under curve of individual peaks.

2.9. Intrinsic Dissolution Studies. IDR of both the CEL crystal habits and their milled fractions was performed in triplicate by the stationary disc method (Wood's assembly) using a USP-24 type 2 apparatus. The intrinsic dissolution studies were performed in 500 mL of three different media: (a) water and (b) pH 12 phosphate buffer and (c) ethanol/water (1:1, v: (v) mixture maintained at 37 ± 0.5 °C at 200 rpm. IDR was calculated from the slope of the initial straight line segment (up to 10 min) in the plot of cumulative amount of drug release (μg/cm^2) vs time (min), as per the procedure described in United States Pharmacopeia (USP). Two milliliters of samples were withdrawn at regular intervals, filtered through 0.22 μm nylon filters, and analyzed by a validated HPLC method fitted with a PDA detector at a wavelength of 252 nm. Surface of the compact was scrapped after experiment and analyzed by XRPD and DSC to identify any solid form transformation during dissolution experiments.

2.10. Wettability Assessment and Surface Free Energy Determination. Advancing contact angles by water, pH 12 phosphate buffer, ethanol/water (1:1), EG and DIM on compacts were measured by the sessile drop method using a Drop Shape Analyzer instrument (FTA 1000, First Ten Angstrom, Virginia, USA). Compact was mounted on a glass slide and a drop of probe liquid was dispensed on them. Video images were captured by the FTA image analyzer using FTA32 software. The contact angle was calculated by fitting mathematical expression to the shape of the drop and then calculating the slope of the tangent to the drop at the liquid−solid−vapor interface line. Further, this contact angle data were utilized for determination of dispersive and polar (both acidic and basic) components of surface free energy using the van Oss−Chaudhury−Good method.[31] All measurements were performed under ambient conditions of 25 ± 2 °C and 55 ± 5% RH, and the average of six measurements is reported.

dx.doi.org/10.1021/cg501084a | Cryst. Growth Des. XXXX, XXX, XXX−XXX

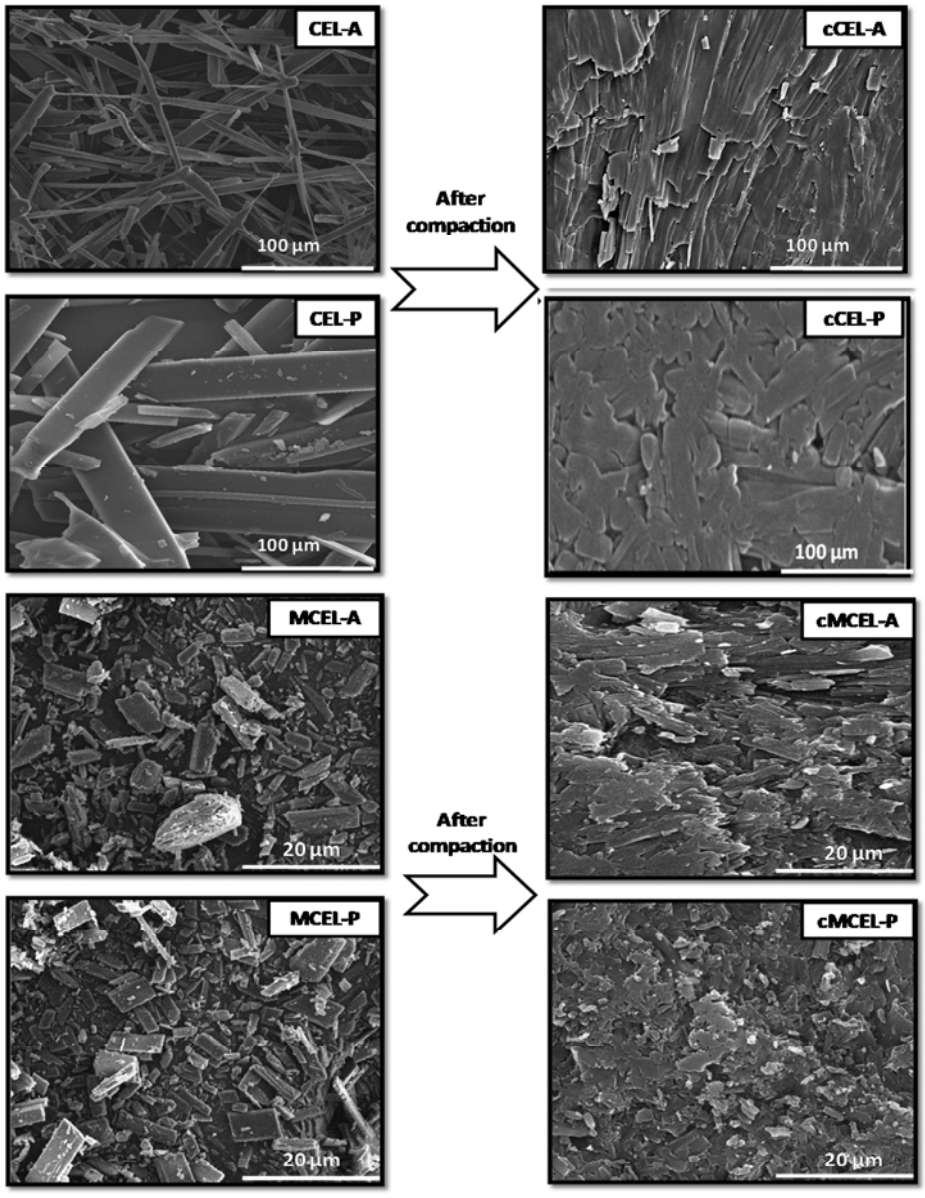

Figure 2. SEM photographs of CEL-A, CEL-P, MCEL-A, MCEL-P and their compacts.

2.11. Statistical Analysis of Data. Statistical significance was determined by Student's *t*-test. Difference was considered significant when the calculated *p* value was less than 0.05.

2.12. Determination of Surface Chemistry Using X-ray Photoelectron Spectroscopy (XPS). X-ray photoelectron spectra were recorded using an ESCA-3000 (VG Scientific Ltd., England) with a 9 channeltron CLAM4 analyzer under a vacuum better than 1×10^{-8} Torr, using Mg−Kα radiation (1253.6 eV) and a constant pass energy of 50 eV. Binding energy range was from 0 to 1100 eV for regions of C 1s, N 1s, O 1s, F 1s, and S 2p with an average peak binding energy of 286.0, 400.9, 533.0, 688.7, and 170.2 eV, respectively. All spectra were corrected for baseline and fitted using Gaussian function. Fitting was performed using PeakFit (V.4.12, SeaSolve Software, Inc., MA, USA). Similar curve fitting treatments were given to all the samples. Surface atomic concentration was determined from integrated peak intensities and the corresponding relative sensitivity factor.

2.13. Crystal Morphology Prediction and Visualization of Surface Molecular Environment of Different Crystallographic Planes. The Bravais-Friedel Donnay-Harker (BFDH) crystal morphology is an approximation based on crystallographic geometrical considerations. The BFDH algorithm, for a given structure, predicts the morphology of a crystal using the corresponding unit cell and symmetry operator information.[32,33] In the present work, BFDH morphology of CEL (Form III, triclinic unit cell) (CSD Reference code: DIBBUL)[34] was predicted using Mercury (version 3.0, Cambridge Crystallographic Data Centre, Cambridge, UK) program to understand the molecular arrangement on the crystal surface.

3. RESULTS

3.1. Solids State Characterization. SEM photographs (Figure 2) confirmed that crystal habits of two batches of CEL crystals used for IDR experiments are different. The aspect ratio for CEL-A was in the range of 12−20 while that for CEL-P was 4−8. However, the milled fraction of plate-shaped (MCEL-P) and acicular (MCEL-A) crystals showed a similar shape with an aspect ratio of 2−6. D_{10}, D_{50}, and D_{90} values of all CEL samples are summarized in Table 1.

SEM photographs also showed the formation of dense compacts in all the samples. The SEM photographs of compacts of CEL-A (cCEL-A), CEL-P (cCEL-P), MCEL-A (cMCEL-A), and MCEL-P (cMCEL-P) suggest that the

dx.doi.org/10.1021/cg501084a | Cryst. Growth Des. XXXX, XXX, XXX−XXX

Table 1. Particle Size Distribution of CEL Sample

diameter (μm)	CEL-A	CEL-P	MCEL-A	MCEL-P
D_{10}	161.8	165.2	3.4	3.1
D_{50}	210.6	212.3	6.2	5.9
D_{90}	262.4	268.9	9.8	10.2

original crystal habit was largely retained in the compacts (Figure 2).

TGA did not show any weight loss in the range of 35−200 °C, indicating an absence of residual solvent in all the samples. DSC analysis revealed similar melting temperature and enthalpy of fusion for powders and their compacts (Figure 3). The onset of melting peaks and enthalpy of fusion for all the samples is summarized in Table 2. Absence of T_g in DSC heating scans and similar values of enthalpy of fusion for all the samples established the absence of solid form transformations during crystallization, milling, and compaction.

XRPD diffractograms (Figure 4) of all the samples showed peaks at 2θ values conforming to Form III of CEL.[34] Variations in relative intensity of peaks between CEL-A and CEL-P can be ascribed to preferred orientation of crystallographic planes.[35,36] Their compacts showed additional changes in peak intensity of some of the prominent peaks when compared to corresponding powder. For example, the intensity of (0 1 0) and their crystallographic parallel planes, increased for both CEL-A and CEL-P after compaction. On the other hand, the intensity of some peaks decreased due to compaction. Thus, compaction further enhanced the preferred orientation, an effect that was more prominent for cCEL-P (Figure 5). The lower degree of preferred orientation of milled fraction than unmilled powders was consistent with previous reports.[26,37] Moreover, compacts of milled fraction did not show obvious signs of change in peak intensities when compared to powder samples.

3.2. Intrinsic Dissolution Studies. IDR experiments were performed in water, pH 12 phosphate buffer, and ethanol/water (1:1). However, because of poor aqueous solubility of CEL, IDR in water was too low to be measured. Intrinsic dissolution profiles of cCEL-A and cCEL-P in pH 12 phosphate buffer are shown in Figure 6a. IDR of cCEL-P was 53.36 ± 6.66 μg/min/cm^2, which is almost 1.5-fold that of cCEL-A (36.50 ± 1.73 μg/min/cm^2). The difference was statistically significant (p = 0.002). However, in the same dissolution medium, the IDRs of cMCEL-P (39.15 ± 2.48 μg/min/cm^2) and cMCEL-A (35.64 ± 5.09 μg/min/cm^2) were not significantly different (p = 0.11) (Figure 6b). Thus, the drug release kinetics from the compacts of the two unmilled habits differed significantly in pH 12 phosphate buffer but were similar for their milled fractions.

Moreover, in ethanol/water (1:1), the IDRs of cCEL-P and cCEL-A were 86.55 ± 7.78 μg/min/cm^2 and 95.04 ± 5.09 μg/min/cm^2, respectively (Figure 7). They were not significantly different (p = 0.131). This differential intrinsic dissolution behavior was further investigated by studying the wettability and determining the surface energetics of these compacts.

3.3. Wettability Assessment and Surface Free Energy Determination. The advancing contact angle of water was significantly higher (p = 0.007) on cCEL-A (78.9° ± 2.2°) than cCEL-P (68.9° ± 2.6°) indicating higher wetting tendency of cCEL-P. When wetting studies were performed using pH 12 phosphate buffer as a probe liquid, advancing contact angles of cCEL-A and cCEL-P were 74.1° ± 1.4° and 64.8° ± 1.2°, respectively. This also indicates better wettability of cCEL-P (p = 0.001) with pH 12 phosphate buffer. However, these differences diminished after milling wherein cMCEL-A and cMCEL-P showed a contact angle of 79.6° ± 1.1° and 77.2° ± 1.2° with water, and 75.5° ± 2.5° and 73.8° ± 2.2° with pH 12 phosphate buffer, respectively (Table 3).

Further, when ethanol/water (1:1) was used as the probe liquid, cCEL-A and cCEL-P had contact angles of 23.6° ± 2.7° and 26.4° ± 2.2°, respectively. This difference was not statistically significant (p = 0.11).

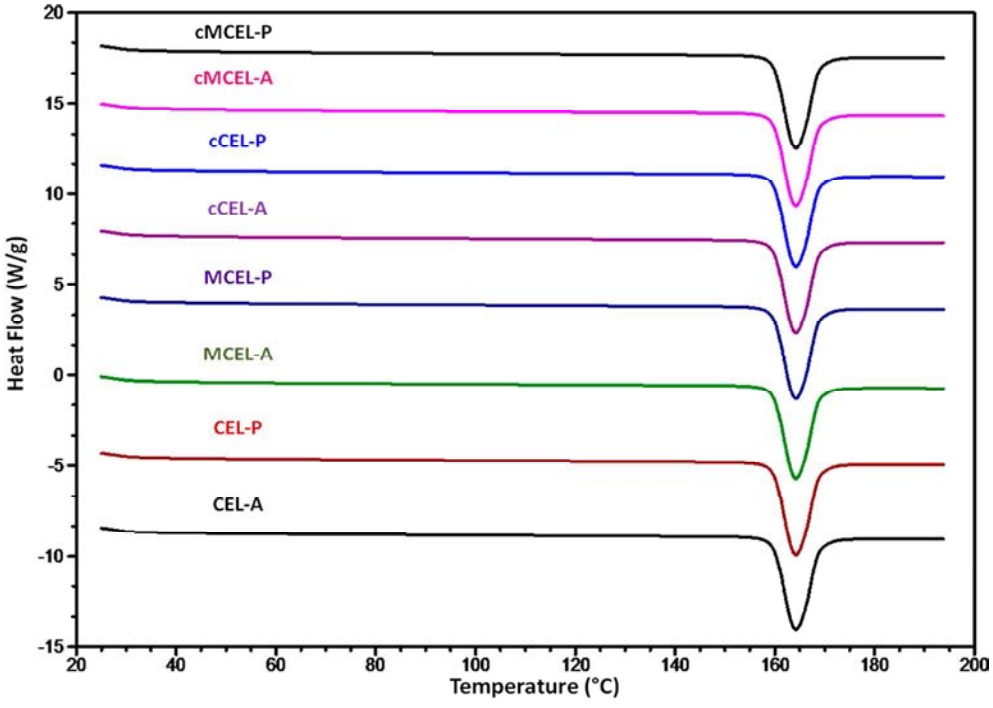

Figure 3. Overlay of DSC heating scans of CEL-A, CEL-P, MCEL-A, MCEL-P and their compacts.

dx.doi.org/10.1021/cg501084a | Cryst. Growth Des. XXXX, XXX, XXX−XXX

Table 2. Thermal Characterization of CEL Samples (n = 3)

property of sample	CEL-A	CEL-P	MCEL-A	MCEL-P	cCEL-A	cCEL-P	cMCEL-A	cMCEL-P
melting point (°C)	162.01 ± 1.82	162.54 ± 2.01	161.13 ± 2.05	161.34 ± 1.82	160.80 ± 1.52	161.20 ± 1.20	160.75 ± 1.73	160.09 ± 2.01
heat of fusion (J/g)	91.23 ± 1.55	91.11 ± 1.58	90.34 ± 2.50	91.66 ± 1.24	90.98 ± 1.37	91.05 ± 2.13	91.89 ± 2.66	90.84 ± 1.70

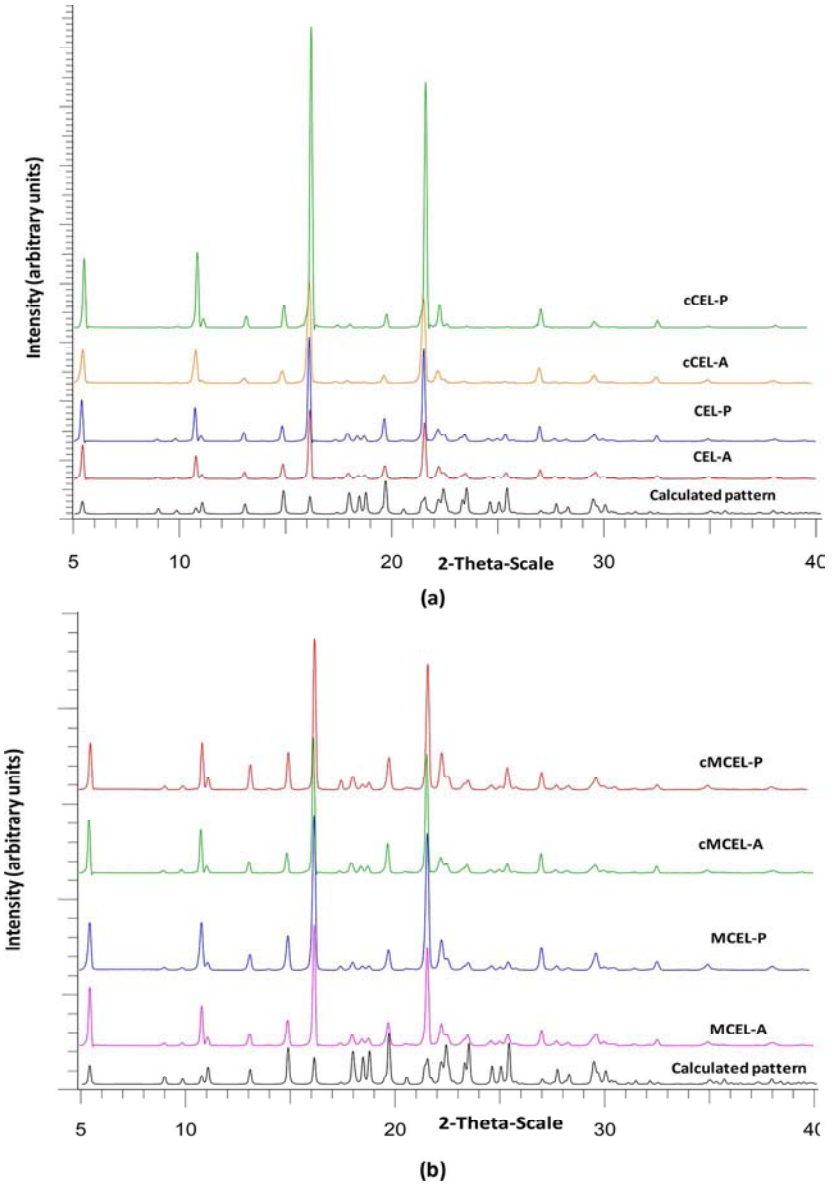

Figure 4. Overlay of XRPD diffractograms of (a) CEL crystal habits and (b) their milled fractions before and after compaction.

The wetting process has three components, namely, adhesion, immersion, and spreading.[38,39] Adhesion is a process in which adhesive forces are found between two phases. Work of adhesion per unit area (W_a) is the work done on the system when solid and liquid, forming an interface of unit area, are separated reversibly.[5,38,40] Immersion is a process in which a solid is covered with a liquid, both of which were initially in contact with a gas without changing the area of liquid−gas interface. The work of immersion per unit area (W_i) is the work done on the system when the process of immersion is carried out.[5,38,40,41] The work of spreading (W_s) is the amount of energy required to spread the liquid on the surface of solid per unit area. The process of spreading requires energy equivalent to the difference between the work of cohesion and the work of adhesion.[40,41] The contact angles of all compacts with pH 12 phosphate buffer and interfacial tension were used to calculate W_a, W_i, and W_s using eqs 2, 3, and 4 respectively, which are derived from the Young's equation.[38,41]

$$W_a = \gamma_{SL} - (\gamma_{SV} + \gamma_{LV}) = -\gamma_{LV}(\cos\theta + 1) \quad (2)$$

$$W_i = 4\gamma_{SL} - 4\gamma_{LV} = -4\gamma_{LV}\cos\theta \quad (3)$$

$$W_s = (\gamma_{SL} + \gamma_{LV}) - \gamma_{SV} = -\gamma_{LV}(\cos\theta - 1) \quad (4)$$

dx.doi.org/10.1021/cg501084a | Cryst. Growth Des. XXXX, XXX, XXX−XXX

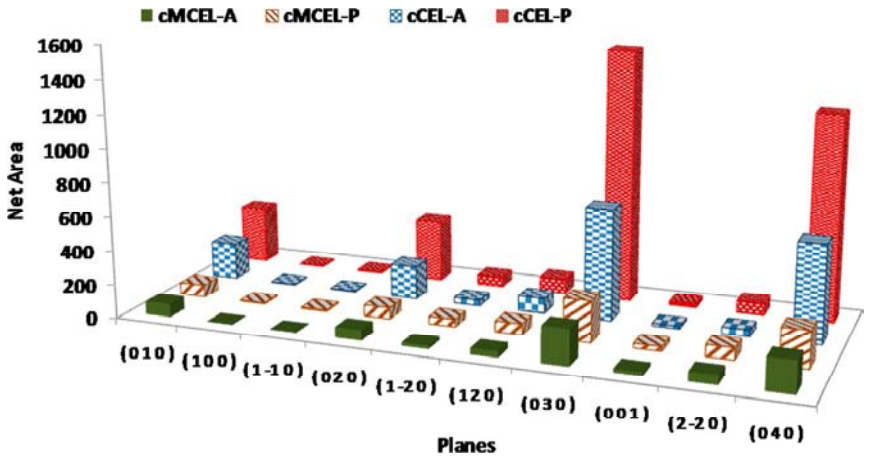

Figure 5. Graphical presentation of XRPD peak intensities of prominent planes in CEL compacts.

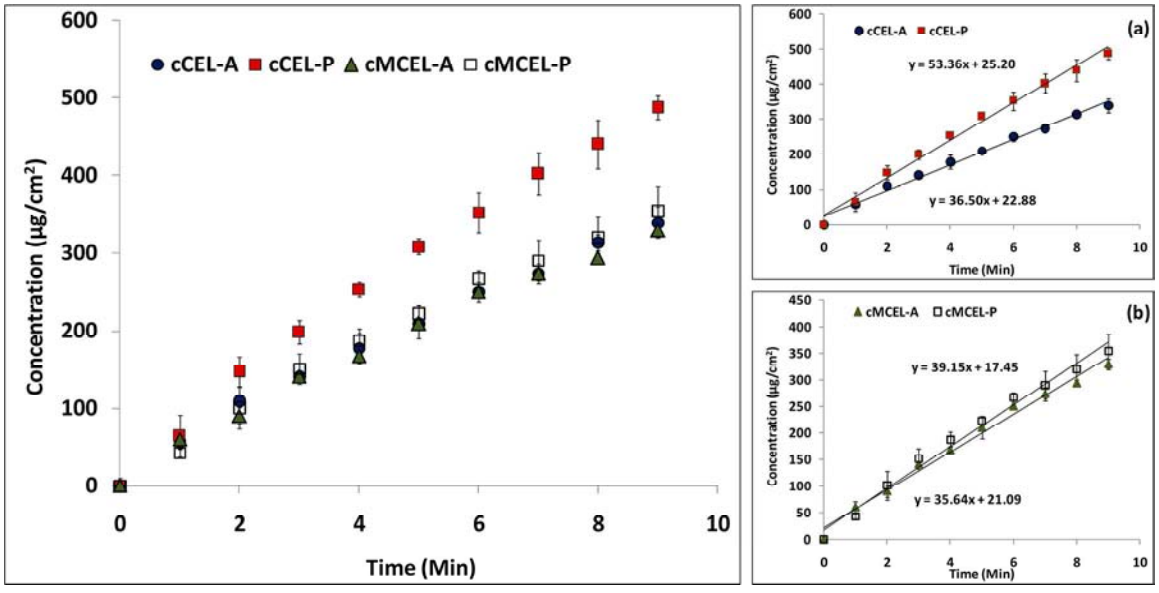

Figure 6. IDR profiles of CEL compacts in pH 12 phosphate buffer. Inset showing greater IDR of cCEL-P over cCEL-A, while there is no difference in IDR of their milled fractions, i.e., cMCEL-A and cMCEL-P.

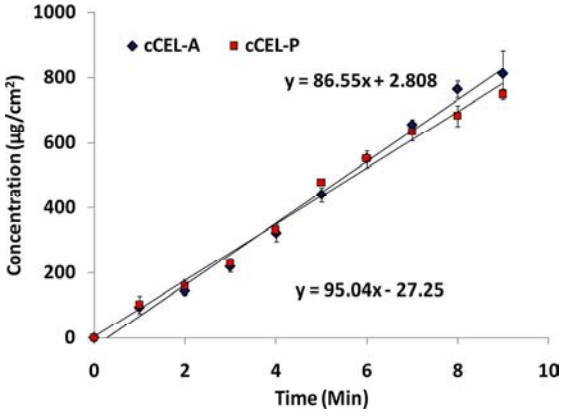

Figure 7. IDR profiles of cCEL-A and cCEL-P in ethanol/water (1:1, v:v).

where θ is the contact angle, γ is interfacial tension, and subscripts LV, SV, and SL refer to the liquid–vapor, solid–vapor, and solid–liquid interfaces, respectively. The thermodynamic driving force, for each process, is indicated by corresponding work value. Considerable difference was found in W_a, W_i, and W_s of cCEL-A and cCEL-P (Table 4). However, no significant difference was observed in W_a, W_i, and W_s of cMCEL-A and cMCEL-P (Table 4). A negative work value indicates the spontaneous nature of the corresponding process. Negative values of W_a and W_i obtained for compacts of both CEL crystal habits indicated the adhesion and immersion process was spontaneous in both cases. On the other hand, the positive value of W_s is indicative of an unfavorable spreading of pH 12 buffer on the surface of these compacts.[38,41]

Moreover, cCEL-A, cCEL-P, cMCEL-A, and cMCEL-P were characterized for their surface free energy using van Oss–Chaudhury–Good method (eq 5).[31,42,43] For this purpose, the advancing contact angle studies were also performed with EG and DIM (Table 3). Contact angle data obtained with water, EG, and DIM were used for calculating surface free energy components. As shown in Table 3, cCEL-P has a higher acidic and basic component, and lower dispersive component of surface free energy as compared to cCEL-A. However, these differences in components of surface free energy diminished in their milled fractions.

dx.doi.org/10.1021/cg501084a | Cryst. Growth Des. XXXX, XXX, XXX–XXX

Table 3. Contact Angle Data and Surface Free Energy Components of CEL Compacts

	contact angle (θ, °)					surface free energy (mJ/m^2)			
sample	water	pH 12 phosphate buffer	water/ethanol (1:1)	EG	DIM	total	dispersive	acidic	basic
cCEL-A	78.9 ± 2.2	74.1 ± 1.4	23.6 ± 2.7	48.5 ± 2.5	17.2 ± 0.5	49.05 ± 1.02	48.55 ± 0.18	5.13 ± 1.25	0.01 ± 0.007
cCEL-P	68.9 ± 2.6	64.8 ± 1.2	26.4 ± 2.2	41.2 ± 1.2	25.6 ± 1.8	46.76 ± 1.35	45.93 ± 0.92	11.68 ± 1.66	0.02 ± 0.01
cMCEL-A	79.6 ± 1.1	75.5 ± 2.5	24.8 ± 2.3	46.2 ± 2.2	25.2 ± 1.8	46.78 ± 1.23	46.05 ± 0.91	4.25 ± 0.23	0.03 ± 0.01
cMCEL-P	77.2 ± 1.2	73.8 ± 2.2	25.6 ± 3.1	47.6 ± 1.3	23.3 ± 0.5	47.34 ± 0.43	46.73 ± 0.23	6.31 ± 1.81	0.02 ± 0.01

Table 4. Values of W_a, W_i, and W_s Calculated for CEL Compacts when pH 12 Phosphate Buffer Used As Probe Liquid

	work values (mJ/m^2)		
sample	W_a	W_i	W_s
cCEL-A	−87.90	−75.61	50.09
cCEL-P	−98.37	−117.51	39.62
cMCEL-A	−86.27	−69.10	51.72
cMCEL-P	−88.25	−77.00	49.74

$$(1 + \cos\theta)\gamma_{LV} = 2\left[\sqrt{\gamma_S^{LW}\gamma_L^{LW}} + \sqrt{\gamma_S^{A}\gamma_L^{B}} + \sqrt{\gamma_L^{A}\gamma_S^{B}}\right] \quad (5)$$

where γ_S, γ^{LW}, γ^A, and γ^B are total, dispersive, acidic, and basic components of surface energies of solids, respectively.

3.4. Determination of Surface Chemistry. XPS spectra showed presence of carbon (C), nitrogen (N), oxygen (O), sulfur (S), and fluorine (F) on the surface of all the powder samples. Peak shape and chemical shift for these elements were similar in these powders, indicating no qualitative differences in them. However, the relative abundance of surface elements shows significant differences (Table 5). As reported earlier by us, the surface of CEL-A sample exhibited a relatively lower concentration of O, N, S and higher concentration of C than CEL-P.[18] However, the surface of MCEL-P exhibited a relatively lower concentration of O, N, S and higher concentration of C and F than CEL-P surface (Table 5). This indicated a lower surface exposure of the hydrophilic $-SO_2NH_2$ group and higher exposure of hydrophobic methyl phenyl and $-CF_3$ group for MCEL-P. Thus, milling altered the surface properties by changing abundance of various crystal facets, governed by their cleavage behavior.

Table 5. Surface Elemental Composition of CEL Samples

	% atomic composition				
crystal sample	O 1s	N 1s	S 2p	F 1s	C 1s
CEL-A[18]	8.48	10.51	10.70	10.12	60.17
CEL-P[18]	9.25	13.13	11.72	10.47	55.41
MCEL-A	9.09	10.92	8.40	10.89	60.70
MCEL-P	8.54	10.13	7.48	12.72	61.13

4. DISCUSSION

Acicular and plate-shaped crystals of CEL, generated by varying the degree of supersaturation and crystallization temperature, were composed of the same solid form, i.e., CEL form III. However, in XRPD, peak intensities differed significantly. CEL-P exhibited significantly higher intensity in a few of the characteristic peaks than CEL-A because of preferred orientation. Compaction augmented the degree of preferred orientation of both the habits as intensity of some of the peaks increased significantly after compaction. The increment in peak intensities of (0 1 0) and its parallel planes was very high in the case of cCEL-P. As expected, a decrease in preferred orientation was observed in compacts of milled fraction. Additionally, compacts of both the milled fractions did not show a significant difference in PXRD peak intensities, in comparison to powder samples.

IDR is defined as the dissolution rate of a pure active substance, where the conditions of surface area, temperature, agitation, pH, and ionic strength of the medium are all constant. It is preferred over powder dissolution for discriminating the biopharmaceutical performance of different solid forms of API.[27] Significant differences were observed in intrinsic dissolution profile of cCEL-A and cCEL-P in pH 12 phosphate buffer.

In contact angle data, cCEL-P exhibited a higher W_a value (−98.37 mJ/m^2) as compared to cCEL-A (−87.90 mJ/m^2), indicating its stronger interaction with aqueous phase. cCEL-P also exhibited a significantly higher W_i (−117.51 mJ/m^2) value as compared to cCEL-A (−75.61 mJ/m^2). The positive W_s value impedes the process of spreading. W_s was found to be positive for both CEL crystal habits, indicating the poor spreadability of aqueous media on their surfaces. cCEL-P, with a lower W_s value (39.62 mJ/m^2), indicated better spreadability of water on its surface than cCEL-A (50.09 mJ/m^2).

Further, the surface free energy can be categorized into dispersive (nonpolar) and hydrogen bonding, i.e., acidic and basic (polar) component.[44] Compacts of CEL crystal habits showed significantly different values for these components. cCEL-P showed relatively lower dispersive component and higher acidic and basic component of surface free energy than for cCEL-A. This may be attributed to the higher exposure of polar groups such as $-SO_2NH_2$ and pyrazole ring on the cCEL-P surface.

The CEL Form III structure described in space group $P\bar{1}$ with unit cell parameters α = 97.62° (7), β = 100.62° (6), γ = 95.95° (4), and a = 10.136 Å (5), b = 16.778 Å (6), c = 5.066 Å (6). The predicted BFDH morphology for CEL Form III (Figure 8a) revealed that {0 1 0} and {1 0 0} families of planes are the principle facets present on the crystal surface. We had previously established surface anisotropy of CEL crystal facets due to differential surface exposure of functional groups.[18] Additionally, face indexation data revealed that the relative abundance of major facets on the surface of CEL-A and CEL-P differed significantly. The percent contribution of a hydrophilic facet {0 1 0} on the surface of CEL-P was higher than CEL-A.[18] In the same paper, we had demonstrated significant differences in wettability, solubility, and oral bioavailability of these two CEL crystal habits (powder) due to their differential surface anisotropy. The overall impact of this differential surface anisotropy was accentuated in compacts due to preferred orientation of crystals as established by differences in peak intensities in the X-ray diffractograms of compacts (Figures 4

dx.doi.org/10.1021/cg501084a | Cryst. Growth Des. XXXX, XXX, XXX−XXX

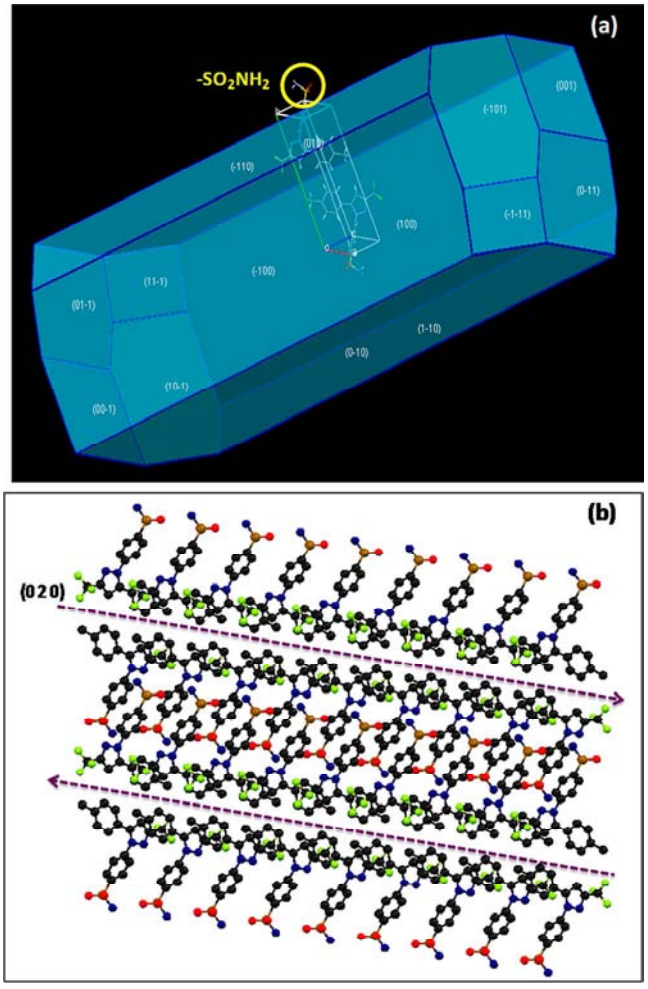

Figure 8. (a) Predicted BFDH morphology for CEL Form III showing the exposure of $-SO_2NH_2$ moieties and (b) visualization of probable cleavage plane (0 2 0) in CEL Form III and its surface molecular environment.

and 5). This preferred orientation leads to a higher exposure of a relatively more hydrophilic {0 1 0} facet on the surface of cCEL-P and contributes to its better wettability and higher IDR.

Interestingly, milled fractions of both crystal habits did not show a significant difference in their intrinsic dissolution profiles. Further, comparative assessment of IDR profiles of cCEL-A and cMCEL-A did not show any significant difference. However, IDR of cCEL-P was significantly higher than cMCEL-P. These results could be explained on the basis of the cleavage pattern during milling and the role preferred orientation.

When particles are subjected to mechanical fracture as a result of comminution, crystals, depending on their shape, will either preferentially break up along their shortest dimension, or along the crystal cleavage plane with low attachment energy.[37,45,46] For CEL form III, {0 2 0} are the most probable cleavage planes because CEL molecules in adjacent layers parallel to (0 2 0) interact through interlayer hydrogen bonding to form hydrogen bonded bilayer. However, hydrogen bonding interactions are absent between the two neighboring bilayers (Figure 8b). Thus, the milling process is likely to expose {0 2 0} planes. Therefore, the functional groups on this facet would predominantly contribute to the surface chemistry in milled powders, which are richer in the relatively hydrophobic $-CF_3$ group and the methyl phenyl ring (Figure 8b). This makes the surface of MCEL-P crystals and their compacts more hydrophobic than CEL-P. On the other hand, the fracture of acicular is easiest along their shortest axis, which is perpendicular to their cleavage plane.[19,37] This led to exposure of both hydrophobic and hydrophilic groups on the surface. As a result, the overall hydrophilicity does not change significantly after milling. This explanation is in line with the crystal surface chemistry determined by XPS (Table 5) and surface free energy data of milled fractions, wherein, cMCEL-A showed a similar polar component of surface free energy as that of cMCEL-P (Table 3). Figure 9 summarizes the comprehensive role of different parameters that are responsible for differential intrinsic dissolution behavior of different CEL samples.

So far the different IDR behaviors have been linked to the surface wettability. To more firmly establish this correlation, we measured IDR using ethanol/water (1:1) as a dissolution medium. The polar component of surface energy of water (51.0 mJ/m^2) is significantly higher than ethanol (2.6 mJ/m^2). On the other hand, water and ethanol have a similar dispersive energy component (21.8 and 18.8 mJ/m^2, respectively). Thus, the addition of ethanol reduces polarity of the medium.[41,47] The less polar ethanol/water (1:1) diminishes the differences in the surfaces and wetting kinetics of both compacts without significantly changing solubility.

USP general chapter ⟨1087⟩ on IDR emphasizes the importance of IDR as a tool to differentiate dissolution performance of solid forms, such as polymorphs, pseudopolymorphs, and amorphous forms. This work establishes that apart from molecular arrangement in crystal lattice, due consideration should also be given to surface molecular environment. In this work, two different crystal habits of the same polymorphic form of CEL (form III) demonstrated significantly different intrinsic dissolution behavior in an aqueous medium due to differential surface molecular environment and wettability.

This observed effect of crystal habit on IDR can also have implications in case of BCS class II drugs. Batch to batch variations in crystal habits can occur during the API crystallization step. Moreover, milling may lead to a change in the relative abundance of different drug crystal surfaces. These changes may lead to unexpected variations in drug release from drug products and their biopharmaceutical performance.

5. CONCLUSIONS

We have demonstrated that the crystal habit significantly affects IDR of CEL form III in pH 12 phosphate buffer. Differential anisotropic surface chemistry of crystal habits coupled with preferred orientation in compacts contributed to this behavior. Higher exposure of hydrophilic facets on the surface of cCEL-P led to their better wettability as compared to cCEL-A in pH 12 phosphate buffer. Such a difference in IDR was eliminated by either using a medium without differential wetting kinetics to cCEL-P and cCEL-A or by milling that diminishes the differential wettability of the two habits. Moreover, this work also demonstrates an example that crystal size reduction cannot only affect powder dissolution but also IDR of drugs. Interpretation of IDR results, apart from molecular arrangement in the crystals, should also give due consideration to the molecular environment on the surface of compacts, which may affect wetting during IDR experiments.

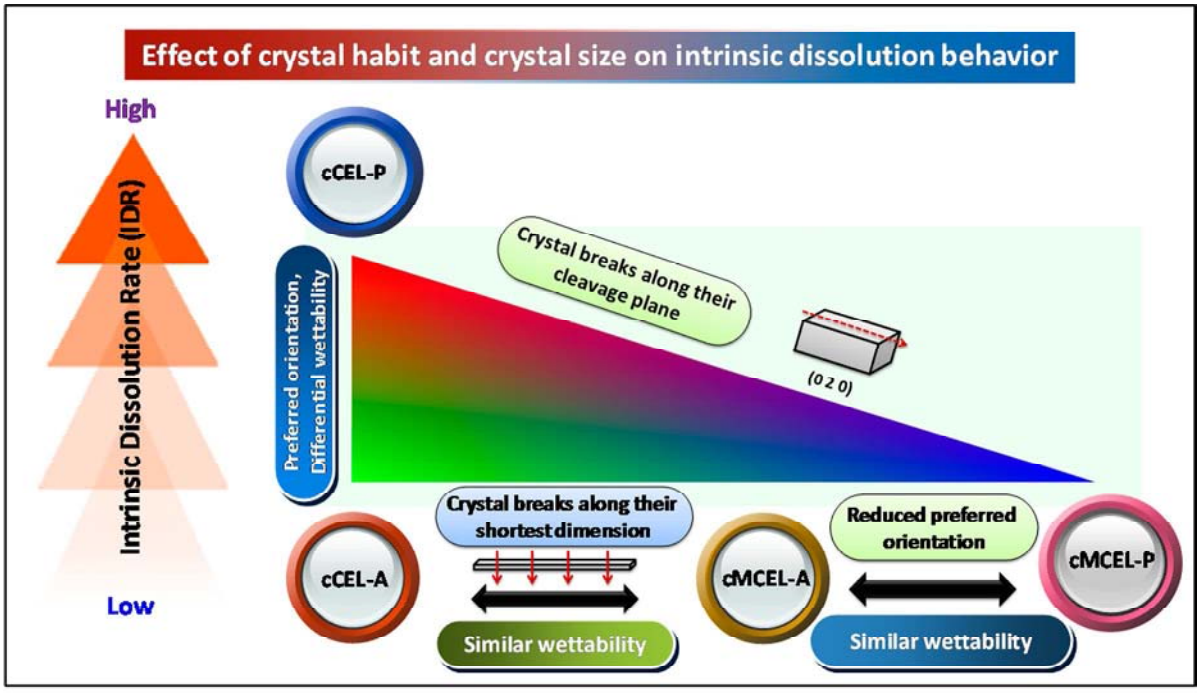

Figure 9. Summarization of the role of different parameters that are responsible for differential intrinsic dissolution behavior of CEL samples.

■ AUTHOR INFORMATION

Corresponding Author

*Tel: +91-172-2214682-86. Fax: +91-172-2214692. E-mail: akbansal@niper.ac.in.

Notes

The authors declare no competing financial interest.

■ ACKNOWLEDGMENTS

We thank the National Chemical Laboratory (NCL), Pune, India, for providing facility of X-ray photoelectron spectroscopy (XPS) and National Institute of Pharmaceutical Education and Research (NIPER), SAS Nagar, for financial support. We are also thankful to Dr. Dimitrios A. Lamprou, University of Strathclyde, UK for his guidance on surface free energy calculations.

■ ABBREVIATIONS

API, active pharmaceutical ingredient; BCS, biopharmaceutical classification system; CEL, celecoxib; CEL-A, acicular crystals of celecoxib; CEL-P, plate-shaped crystals of celecoxib; IDR, intrinsic dissolution rate; XPS, X-ray phaotoelectron spectroscopy

■ REFERENCES

(1) Mullin, J. W. *Crystallization*, 4 ed.; Butterworth-Heinemann: Oxford, 2001; pp 181−284.

(2) Perumal, O.; Podaralla, S. Role of Preformulation in Development of Solid Dosage Forms. In *Pharmaceutical Manufacturing Handbook:Production and Processes*; Gad, S. C., Ed.; John Wiley & Sons: NJ, 2008; Vol. *10*, pp 936.

(3) Sun, C. C. *J. Pharm. Sci.* **2008**, *98*, 1671−1687.

(4) Blagden, N.; de Matas, M.; Gavan, P. T.; York, P. *Adv. Drug Delivery Rev.* **2007**, *59*, 617−30.

(5) Buckton, G. *J. Adhes. Sci. Technol.* **1993**, *7*, 205−219.

(6) Buckton, G.; Bulpett, R.; Verma, N. *Int. J. Pharm.* **1991**, *72*, 157−162.

(7) Burt, H. M.; Mitchell, A. *Int. J. Pharm.* **1980**, *5*, 239−251.

(8) Danesh, A.; Connell, S. D.; Davies, M. C.; Roberts, C. J.; Tendler, S. J. B.; Williams, P. M.; Wilkins, M. *Pharm. Res.* **2001**, *18*, 299−303.

(9) Heng, J. Y. Y.; Bismarck, A.; Lee, A. F.; Wilson, K.; Williams, D. R. *Langmuir* **2006**, *22*, 2760−2769.

(10) Heng, J. Y. Y.; Bismarck, A.; Lee, A. F.; Wilson, K.; Williams, D. R. *J. Pharm. Sci.* **2007**, *96*, 2134−44.

(11) Li, T.; Liu, S.; Feng, S.; Aubrey, C. E. *J. Am. Chem. Soc.* **2005**, *127*, 1364−1365.

(12) Mitchell, A. G.; Milaire, B. L.; Saville, D. J.; Griffiths, R. V. *J. Pharm. Pharmacol.* **1971**, *23*, 534−5.

(13) Prasad, K. V. R.; Ristic, R. I.; Sheen, D. B.; Sherwood, J. N. *Int. J. Pharm.* **2002**, *238*, 29−41.

(14) Prestidge, C. A.; Tsatouhas, G. *Int. J. Pharm.* **2000**, *198*, 201−212.

(15) Tiwary, A. K. *Drug Dev. Ind. Pharm.* **2001**, *27*, 699−709.

(16) Sun, C.; Grant, D. J. W. *J. Pharm. Sci.* **2001**, *90*, 569−579.

(17) Banga, S.; Chawla, G.; Varandani, D.; Mehta, B. R.; Bansal, A. K. *J. Pharm. Pharmacol.* **2007**, *59*, 29−39.

(18) Modi, S. R.; Dantuluri, A. K.; Puri, V.; Pawar, Y. B.; Nandekar, P.; Sangamwar, A. T.; Perumalla, S. R.; Sun, C. C.; Bansal, A. K. *Cryst. Growth Des.* **2013**, *13*, 2824−2832.

(19) Modi, S. R.; Khomane, K. S.; Bansal, A. K. *Int. J. Pharm.* **2014**, *460*, 189−195.

(20) Kumar, D.; Shastri, N. R. *Cryst. Growth Des.* **2013**, *14*, 326−338.

(21) Shah, U. V.; Olusanmi, D.; Narang, A. S.; Hussain, M. A.; Gamble, J. F.; Tobyn, M. J.; Heng, J. Y. *Int. J. Pharm.* **2014**, *472*, 140−147.

(22) Mosharraf, M.; Nyström, C. *Int. J. Pharm.* **1995**, *122*, 35−47.

(23) Wood, J. H.; Syarto, J. E.; Letterman, H. *J. Pharm. Sci.* **1965**, *54*, 1068−1068.

(24) Agrawal, S.; Ashokraj, Y.; Bharatam, P. V.; Pillai, O.; Panchagnula, R. *Eur. J. Pharm. Sci.* **2004**, *22*, 127−44.

(25) Chow, A. H. L.; Hsia, C. K.; Gordon, J. D.; Young, J. W. M.; Vargha-Butler, E. I. *Int. J. Pharm.* **1995**, *126*, 21−28.

(26) Tenho, M.; Heinänen, P.; Tanninen, V. P.; Lehto, V. P. *J. Pharm. Biomed. Anal.* **2007**, *43*, 1315−1323.

(27) Yu, L. X.; Carlin, A. S.; Amidon, G. L.; Hussain, A. S. *Int. J. Pharm.* **2004**, *270*, 221−227.
(28) Ho, R.; Wilson, D. A.; Heng, J. Y. Y. *Cryst. Growth Des.* **2009**, *9*, 4907−4911.
(29) Chan, H.-K.; Grant, D. J. *Int. J. Pharm.* **1989**, *57*, 117−124.
(30) Šehić, S.; Betz, G.; Hadžidedić, Š.; El-Arini, S. K.; Leuenberger, H. *Int. J. Pharm.* **2010**, *386*, 77−90.
(31) Van Oss, C. J.; Good, R. J.; Chaudhury, M. K. *Langmuir* **1988**, *4*, 884−891.
(32) Docherty, R.; Clydesdale, G.; Roberts, K.; Bennema, P. *J. Phys. D: Appl. Phys.* **1991**, *24*, 89.
(33) Hammond, R. B.; Pencheva, K.; Roberts, K. J. *Cryst. Growth Des.* **2006**, *6*, 1324−1334.
(34) Dev, R. V.; Rekha, K. S.; Vyas, K.; Mohanti, S. B.; Kumar, P. R.; Reddy, G. O. *Acta Crystallogr.* **1999**, *55*, No. IUC9900161.
(35) Koivisto, M.; Virjonen, T.; Heikkilä, T.; Lehto, V. P. *J. Pharm. Biomed. Anal.* **2004**, *36*, 559−564.
(36) Leventouri, T. *Physica C: Superconductivity* **1997**, *277*, 82−86.
(37) Ho, R.; Naderi, M.; Heng, J. Y. Y.; Williams, D. R.; Thielmann, F.; Bouza, P.; Keith, A. R.; Thiele, G.; Burnett, D. J. *Pharm. Res.* **2012**, *29*, 1−11.
(38) Buckton, G. *Int. J. Pharm.* **1988**, *44*, 1−8.
(39) Laad, P.; Shete, G.; Modi, S. R.; Bansal, A. K. *Eur. J. Pharm. Sci.* **2013**, *49*, 109−116.
(40) Young, S. A.; Buckton, G. *Int. J. Pharm.* **1990**, *60*, 235−241.
(41) Puri, V.; Dantuluri, A. K.; Kumar, M.; Karar, N.; Bansal, A. K. *Eur. J. Pharm. Sci.* **2010**, *40*, 84−93.
(42) Wu, S. *J. Polym. Sci.* **1971**, *34*, 19−30.
(43) Mall, S.; Buckton, G.; Gregori, T.; Rawlins, D. *J. Phys. Chem.* **1995**, *99*, 8356−8361.
(44) Fowkes, F. M. *Adv. Chem. Ser.* **1964**, *43*, 99−111.
(45) Heng, J. Y. Y.; Thielmann, F.; Williams, D. R. *Pharm. Res.* **2006**, *23*, 1918−1927.
(46) Shariare, M. H.; Blagden, N.; Matas, M.; Leusen, F. J. J.; York, P. *J. Pharm. Sci.* **2012**, *101*, 1108−19.
(47) Zografi, G.; Tam, S. S. *J. Pharm. Sci.* **1976**, *65*, 1145−1149.